Frequency Regulation Feasible Region Assessment and Optimization of Wind Farm Based on Data-Driven Model Predictive Control

Jiachen Liu, Zhongguan Wang*, Li Guo, Chengshan Wang
School of Electrical and Information Engineering
Tianjin University
Tianjin, China
wang_zg@tju.edu.cn

Shunqi Zeng, Minghui Chen
Guangzhou Power Supply Bureau
China Southern Power Grid Co.
Guangzhou, China
peishunqi@163.com

***Abstract*—With the integration of large-scale wind turbines (WTs) into grids via electronic interfaces, power system operators have necessitated frequency support from wind farms. Due to the large number of WTs and their complex dynamic characteristics, it is necessary to assess the primary frequency regulation (PFR) capability and construct feasible region of wind farms. In order to cope with the problems of incomplete parameters, analytical solving complexity and the coupling influence of power system regulation characteristics, this paper develops a data-driven state space mapping linear model predictive control (MPC) to assess the maximum PFR capability of wind farms and reasonably distribute coefficients to WTs. Besides, a coordinated iteration framework between dispatching center and wind farms is proposed to further optimize the wind farm regulation feasible region. The simulation results verify that the proposed method has the advantages of independence from physical parameters, fast analytical solution, and lower requirements of training samples on limited scenarios.**

***Index Terms*—Data-driven, droop coefficient, frequency regulation, Koopman operator, state space mapping, wind farm.**

I. INTRODUCTION

With the rapid increase of WT installed capacity, power system PFR is confronted with significant problems [1]. WTs connect with power systems via converters, which leads to the decoupling of rotor speed and system frequency [2]. On the other hand, most WTs operate at maximum power point tracking (MPPT) mode without reverse capability, which further deteriorates frequency stability [3]. To cope with these challenges, it has reached a consensus that power systems need to incorporate WTs in frequency regulation, especially in PFR process.

Variable speed WTs usually participate in PFR accoding to two control schemes, i.e. converter control and pitch angle control. Compared to the pitch angle control scheme, the electronic converter has the advantage of responding rapidly and low cost, and hence becomes a more efficient method [4]. This approach emulates the droop characteristic of conventional generators by utilizing the stored kinetic energy in WTs [5], [6]. The authors of [7] validate that provision of droop characteristics by WTs can improve the quasi-steady state of frequency and frequency nadir. Based on rotor speed status, an adaptive droop coefficient control method is developed in [8] to avoid WT tripping-off incidents. Nevertheless, these approaches mostly focus on the individual WT control.

As a grid-connected entity, a wind farm should reasonably dispatch power among WTs and provide unitary droop characteristics during a PFR process. With different WT status and wind speed conditions, the regulation capability of a wind farm will dynamically change [9]. Considering the security of WT rotor speed, it is important to assess the optimal droop coefficient feasible region of wind farms in different operation status, and report to the grid dispatching center, which helps dispatchers to analyze the frequency stability and perform unit commitment considering dynamic security. Usually, based on a dynamic physical model, the optimal boundary of droop coefficient feasible region can be analytically calculated. Ref. [10] utilizes an analytical function of wind speed condition and WT rotor speed to assess the limited boundary of wind farm droop coefficient. The authors in [11] propose an enhanced steady-state power flow method based on timing simulation to assess the contribution of voltage source converter-based high voltage direct current transmission (VSC-HVDC) wind farm to frequency regulation. In [12], the droop coefficient boundary is expressed by a linear time-vary function of wind speed. A mixed integer linear programming method is developed in [13] to assess the feasible region of regulation coefficients, which takes frequency response and economic constraints into consideration. The authors of [14] make a tradeoff between economic benefit and reserve active power to assess

This work was supported in part by the Technology Project of China Southern Power Grid Co., Ltd under Grant GDKJXM20220183, and in part by the National Natural Science Foundation of China under Grant 52007129.

maximum droop coefficient of wind farms. However, the above traditional physical approaches rely heavily on parameter accuracy and model completeness [15]. With imprecise parameters, the assessed results inevitably deteriorate. Meanwhile, the assessment of the droop coefficient feasible region is a nonconvex optimal problem constrained by nonlinear dynamic equations, and the distribution scheme of coefficient among WTs should also be considered, and hence the fast analytical solution is difficult. In general, timing simulation methods can be used to solve this problem and obtain the coefficient boundary [16], [17], but the solution efficiency interferes with its online application.

Compared to the aforementioned traditional model-based methods, data-driven methods have attracted much attention from scholars since they directly use the input and output information of a real system to construct an equivalent model [18]. The authors of [19] develop an improved elastic back-propagation neural network method to forecast frequency variation of a wind farm integrated system. In [20], an artificial neural network model is developed to fit the PFR dynamic model and assess the frequency regulation capability of wind farms. Ref. [21] proposes a deep reinforcement learning method to construct a frequency regulation model of wind farms and assess the droop coefficient in real-time. Nevertheless, the above data-driven methods lack physical interpretability, which makes it difficult to accurately fit the nonlinear dynamical process of wind farm PFR.

To cope with the problem, a data-driven MPC is an promising scheme, since it has the advantage of combining dynamic mechanism process. The authors of [22] construct a MPC model by long short-term memory units and convolutional neural networks. However, due to the strong nonlinear characteristic, the model is solved by a heuristic optimal algorithm, instead of the analytic method, which suffers from long solving time and unstable results. Owing to global linearization, the Koopman operator theory (KOT) is widely used in fitting a nonlinear dynamic model [23]. Based on KOT, a nonlinear dynamic model can be mapped onto a global linear pattern in augmented state space without loss of accuracy, and a linear operator matrix can be estimated by data-driven training [24], [25]. In this way, constructing a convex optimization model with accurate data-driven linear MPC is possible.

In addition, it should be emphasized that each wind farm PFR capability exists coupling relationship in a power system, which is ignored in most existing research. Specifically, when wind farms obtain an assessment result and report it to the grid dispatcher, the overall frequency regulation capability of the system will be reinforced, which further extends the droop coefficients feasible region of each wind farm in turn. Therefore, in order to obtain the optimal coefficient boundary of wind farms, it is necessary to carry out a coordinated iteration scheme between the grid dispatch center and wind farms.

To fill the gaps in the existing research, this paper develops a data-driven and state space mapping linear MPC method to construct a wind farm PFR capability assessment model. The assessed result of each wind farm model is reported to the grid dispatch center, and the center updates system coefficient and feed it back to wind farms. By executing the coordinated iteration, the optimal feasible region of wind farms can be obtained. To the best of the author's knowledge, the main contributions of this paper can be concluded as follows:

1) A data-driven state space mapping linear MPC model of wind farm PFR is proposed, which is independent of WT parameters and reduces the requirement for historical samples by global linearization.

2) A convex PFR capability assessment model of wind farms is constructed based on the data-driven MPC, which has the advantages of fast analytical solving and optimal coefficient distribution among WTs.

3) A coordinated iteration assessment framework between grid dispatching center and wind farms is proposed, which completely exploits the PFR capability.

The remainder of this paper is organized as follows: Section II introduces a physical-based nonlinear MPC assessment model and coordinated iteration framework. Section III develops coordinated assessment method based on state space mapping and data-driven linear MPC, and the effectiveness of PFR capacity assessment is validated in Section IV. Finally, Section V concludes the paper.

II. Physical-Based Nonlinear MPC Assessment Model and Coordinated Iteration Framework

As a theoretical basis of the proposed data-driven MPC assessment method, a physical-based MPC model with a coordinated assessment framework is introduced in this section.

A. Continuous-Time Differential Dynamic Model of PFR

WTs capture the kinetic energy from the air and store it in wind blades. The mechanical power of WT can be expressed as follows [25]:

$$P_{m,i,n} = \frac{1}{2}\rho S v_{w,i,n}^3 C_{p,i,n}\left(\lambda_{i,n}, \beta_{i,n}\right) \tag{1}$$

where $P_{m,i,n}$ denotes the mechanical power of n-th WT in i-th wind farm, ρ denotes the air density, S denotes the swept area of WT blades, $v_{w,i,n}$ denotes the wind speed of n-th WT in i-th wind farm, and $C_{p,i,n}\left(\lambda_{i,n}, \beta_{i,n}\right)$ denotes the power coefficient of n-th WT in i-th wind farm [25], i.e.,

$$C_{p,i,n}\left(\lambda_{i,n}, \beta_{i,n}\right) = 0.22\left(\frac{116}{\sigma_{i,n}} - 0.4\beta_{i,n} - 5\right)e^{\frac{-12.5}{\sigma_{i,n}}} \tag{2}$$

where $\lambda_{i,n} = r_{i,n}\omega_{i,n}(t) / v_{w,i,n}$ denotes the ratio of blade tip speed to wind speed, $r_{i,n}$ and $\beta_{i,n}$ denotes the blade radius and blade pitch angle of n-th WT in i-th wind farm, and

$$\frac{1}{\sigma_{i,n}}=\frac{1}{\lambda_{i,n}+0.08\beta_{i,n}}-\frac{1}{\beta_{i,n}^3+1} \tag{3}$$

In a PFR process, operation mode of WT is switched to droop control, and causes a mismatch between the electrical and mechanical torque. The electro-mechanical transient process is represented as

$$\dot{\omega}_{i,n}=\frac{1}{J_c}\cdot(T_{m,i,n}-T_{e,i,n})=\frac{1}{J_c}\cdot(\frac{P_{m,i,n}}{\omega_{i,n}}-\frac{P_{e,i,n}}{\omega_{i,n}}) \tag{4}$$

where $\omega_{i,n}$ denotes the rotor speed of *n*-th WT in *i*-th wind farm, $T_{m,i,n}$ and $T_{e,i,n}$ denotes the mechanical torque and electrical torque of *n*-th WT in *i*-th wind farm, $P_{m,i,n}$ and $P_{e,i,n}$ denotes the active power output of *n*-th WT in *i*-th wind farm, and J_{c} denotes the rotational inertia of the WT.

After a severe power fluctuation, if system frequency exceeds the pre-set dead zone, generators will regulate the active power output and participate in PFR. Both thermal units and WTs regulate the power by droop control, which can be represented as

$$\Delta P_G=(K_{f,th}+K_f)(f^*-f)=\sum_{i=1}^{l}\Delta P_{e,i}+\sum_{j=1}^{h}\Delta P_{th,j} \tag{5}$$

$$\Delta P_{e,i}=K_{f,i}(f^*-f) \tag{6}$$

$$K_f=\sum_{i=1}^{l}K_{f,i} \tag{7}$$

$$\Delta P_{th,j}=K_{f,th,j}(f^*-f) \tag{8}$$

$$K_{f,th}=\sum_{j=1}^{h}K_{f,th,j} \tag{9}$$

where ΔP_G denotes the total active power output adjustment in the system, $\Delta P_{th,j}$ and $\Delta P_{e,i}$ denote the active power output adjustment of the *j*-th thermal power plant and the *i*-th wind farm, $K_{f,th,j}$ and $K_{f,i}$ denote the droop coefficients of the *j*-th thermal power plant and the *i*-th wind farm, l and h denote the number of thermal power plants and wind farms in the system, $K_{f,th}$ and K_f denote the total droop coefficients of thermal power plants and wind farms, f^* denotes the nominal frequency, and f denotes the real frequency.

In this paper, the system frequency dynamic response process is expressed as a first-order inertial function, which can be expressed as (10). To guarantee the assessment results can apply to all scenarios, we set a most acceptable power fluctuation at the beginning of PFR, and implement iteration assessment. In this way, the assessed results can guarantee WT security in all acceptable power fluctuation scenarios.

$$\frac{2H}{f_n}\frac{\mathrm{d}f}{\mathrm{d}t}=\Delta P_G-\Delta P_L=K_{f,sys}(f^*-f)-\Delta P_L \tag{10}$$

$$K_{f,sys}=K_{f,th}+K_f \tag{11}$$

where H denotes the inherent inertia of the system, $K_{f,sys}$ denotes the total droop coefficient of the system, and ΔP_L denotes the load disturbance.

To provide a stable regulation characteristic, $K_{f,i}$ should be a constant in one PFR process, and the power output of the *i*-th wind farm can be expressed as

$$P_{e,i}=\sum_{n=1}^{N_i}P_{e,i,n}=\Delta P_{e,i}+P_{m,i}^{in}=K_{f,i}(f^*-f)+\sum_{n=1}^{N_i}P_{m,i,n}^{in} \tag{12}$$

$$P_{m,i}^{in}=\sum_{n=1}^{N_i}P_{m,i,n}^{in} \tag{13}$$

$$P_{e,i,n}=P_{m,i,n}^{in}+K_{f,i,n}(f^*-f) \tag{14}$$

where $P_{m,i}^{in}$ and $P_{e,i}$ denotes the initial mechanical power and power output of the *i*-th wind farm, N_i denotes the number of WTs in the *i*-th wind farm, $P_{m,i,n}^{in}$ and $P_{e,i,n}$ denotes the initial mechanical power and power output of the *n*-th WT in the *i*-th wind farm, and $K_{f,i,n}$ denotes the droop coefficient of the *i*-th WT in the *i*-th wind farm.

B. Coordinated Discrete-Time Algebraic MPC Assessment Model

1) Wind Farm Model

In order to carry out an analytic solving of PFR process, the original dynamic model is usually derived into an algebra form by the finite difference method. The discrete algebraic form of system frequency (8) can be rewritten as

$$f(t+1)=f(t)+\frac{f_{\mathrm{n}}^*T}{2H}[K_{f,sys}(f^*-f(t))-\Delta P_L] \tag{15}$$

where T denotes the sampling period, and $\bullet(t)$ denotes the value at time step *t*.

Similarly, the discrete algebraic form of rotor transient is

$$\omega_{i,n}(t+1)=\frac{T\cdot(P_{m,i,n}(t)-P_{e,i,n}(t))}{J_{\mathrm{c}}\cdot\omega_{i,n}(t)}+\omega_{i,n}(t) \tag{16}$$

It should be noted that the PFR capability of wind farms is assessed before the actual PFR process, and the assessment is rolling implemented at the minute level. Each rolling prediction horizon of MPC is a multi-step dynamical and time-coupling process, and hence we can utilize the time indicator "*t*" to enumerate control points directly. In order to provide stable frequency support, the wind farm/WT droop coefficient should be a constant value during the PFR. Meanwhile, droop coefficient will influence the dynamic process of rotor speed according to (14) and (16). Therefore, for each wind farm, the MPC optimization problem should assess the boundary of wind farm droop coefficient feasible region in the whole PFR process by (17-a) with the constraints of rotor speed in (17-h) and physical dynamic evolution in (7), (9), (11), (13), (15), (16) and (17-b)-(17-g) in each dynamic control step. Hence, the above process is difficult to adopt a

classical receding horizon formulation, shown in (17), and the feasible region can be denoted by $[0, K_{f,i}^*]$, in which $K_{f,i}^*$ denotes the optimal assessment results.

$$\text{for all } n \in \{1,2,\cdots,N_i\}, t \in \{1,2,\cdots,m\}$$

$$\mathsf{U}_i^* = \arg\max_{\{K_{f,i,n}\}} K_{f,i} = \sum_{n=1}^{N_i} K_{f,i,n} \tag{17-a}$$

$$\text{s.t. } P_{m,i,n}(t) = \frac{1}{2}\rho S v_{w,i,n}^3 C_{p,i,n}\left(\lambda_{i,n}(t), \beta_{i,n}(t)\right) \tag{17-b}$$

$$C_{p,i,n} = 0.22\left(\frac{116}{\sigma_{i,n}(t)} - 0.4\beta_{i,n}(t) - 5\right)e^{\frac{-12.5}{\sigma_{i,n}(t)}} \tag{17-c}$$

$$\frac{1}{\sigma_{i,n}(t)} = \frac{1}{\lambda_{i,n}(t) + 0.08\beta_{i,n}(t)} - \frac{1}{\beta_{i,n}^3(t) + 1} \tag{17-d}$$

$$\lambda_{i,n}(t) = r_{i,n}\omega_{i,n}(t) / v_{w,i,n} \tag{17-e}$$

$$P_{e,i}(t) = \sum_{n=1}^{N_i} P_{e,i,n}(t) = K_{f,i}(f^* - f(t)) + P_{e,i}^{in} \tag{17-f}$$

$$P_{e,i,n}(t) = P_{m,i,n}^{in} + K_{f,i,n}(f^* - f(t)) \tag{17-g}$$

$$\omega_{\min,i,n} \le \omega_{i,n}(t) \le \omega_{\max,i,n} \tag{17-h}$$

$$K_{f,i,n} \ge 0 \tag{17-i}$$

$$\text{and (7), (9), (11), (13), (15), (16)}$$

where m denotes the number of discrete control points in a prediction horizon, $\omega_{\min,i,n}$ and $\omega_{\max,i,n}$ denote the minimum and maximum limit speed of the n-th WT in the i-th wind farm, and U_i^* denotes the optimal $K_{f,i,n}$ set in the i-th wind farm with largest $K_{f,i}$.

2) Grid Dispatching Side

The system total droop coefficient increases with the assessment results reported from wind farms, and (11) can be rewritten as

$$K_{f,sys}(s+1) = K_f(s) + K_{f,th} = \sum_{i=1}^{l} K_{f,i}(s) + \sum_{j=1}^{h} K_{f,th,j} \tag{18}$$

where $\bullet(s)$ denotes the value at iteration step s.

$$\begin{cases} \text{Equ. (18)} \\ K_{f,1}(s+1) = \mathsf{U}_1^*\left(K_{f,1},\ K_{f,sys}(s+1)\right) \\ K_{f,2}(s+1) = \mathsf{U}_2^*\left(K_{f,2},\ K_{f,sys}(s+1)\right) \\ \vdots \\ K_{f,l}(s+1) = \mathsf{U}_l^*\left(K_{f,l},\ K_{f,sys}(s+1)\right) \end{cases} \tag{19}$$

By observing the assessment model on the wind farm side, it can be proved that the maximum PFR capability of each wind farm is further enhanced with an updated system coefficient, and hence an alternative iteration method in (19) is adopted to search for the optimal coefficient boundary of each wind farm. It should be noted that the wind farm coefficient assessment in one iteration can be parallel executed:

It is well known that a monotone bounded series of numbers must converge. Therefore, if we validate system droop coefficients series in the iteration process is monotone bounded series, we can validate that the coordinated iteration is convergent.

1) Monotonicity: In the first assessment, system droop coefficient is only provided by synchronous generators, and the assessment results of wind farms are reported to the dispatching center and increase system droop coefficient. The augment of system PFR capability will reduce the frequency deviation of each step in PFR. In other words, if using the assessed coefficients before iteration under this case, the WT rotor speed after PFR can be kept within the boundary. Based on (14) and (16), WTs can reduce the distance between rotor speed after PFR and constraint boundaries by increasing the droop coefficient. In this way, the assessed droop coefficients of each wind farm will increase with the augmented system droop coefficient. With updated wind farm coefficients, the system droop is further increased, and hence the iterative results of wind farm are monotone series.

2) Boundedness: From the perspective of conservation of energy, wind farm PFR capability comes from the kinetic energy in WT blades which must have an upper limit. In this way, system droop must have a supremum when all WT kinetic energy is fully exploited.

To sum up, the system and wind farms' droop coefficient in the coordinated iteration is monotonic bounded series which must converge. If $K_{f,i}(S)$ and $K_f(S)$ satisfy convergence conditions in (20), the coordinated iteration finishes and obtains the optimal feasible region of wind farm droop coefficient.

$$\begin{cases} \left|K_f(S+1) - K_f(S)\right| < \delta_1 \\ \left|K_{f,i}(S+1) - K_{f,i}(S)\right| < \delta_2, \text{ for all } i \in \{1,2,\cdots,l\} \end{cases} \tag{20}$$

where δ_1 and δ_2 denote the tolerance, and S denotes the step number of convergence.

To explicitly express, we take the i-th wind farm as a representative and exhibit the coordinated iteration process between the wind farm and grid dispatching center, as shown in Fig. 1. The results of iterative assessment should be unique, and the conclusion can be easily proved by using reduction to absurdity.

Nevertheless, the above coordinated algebraic MPC assessment model in (19) is a nonconvex optimal problem, which is difficult to solve analytically, suffers from low efficiency and is unsuitable for online application. Meanwhile, the assessment accuracy of the physical-based model is also interfered by the inaccurate parameters and model completeness.

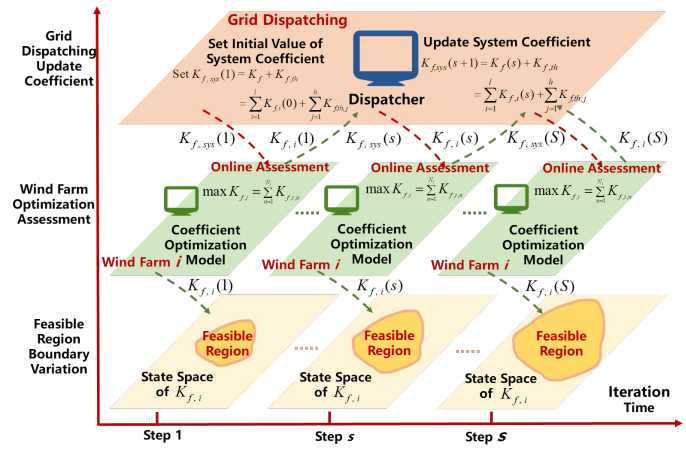

Fig. 1. Coordinated iteration framework of PFR capability assessment.

III. Coordinated Assessment Method Based on State Space Mapping and Data-Driven Linear MPC

To cope with the challenges of physical-based method, this section derives a data-driven state space mapping linear MPC model based on the Koopman operator, and assesses the optimal feasible region of wind farms based on the coordinated iteration.

A. Data-Driven State Space Mapping Linear Model

1) Linear MPC Model Based on State Space Mapping

Based on the KOT, a nonlinear algebraic equation can be mapped onto a global linear form in an infinite-dimensional Hilbert state space without loss of accuracy. In practice, it is sufficient to augment the state space to an appropriate number, instead of infinite dimension, to highly fit the nonlinear relationship in the original state space. Owing to the global linearization, the historical samples of wind farms are unnecessary to cover the limited operation scenarios. Fig. 2 exhibits the schematic diagram of the KOT-based state space mapping.

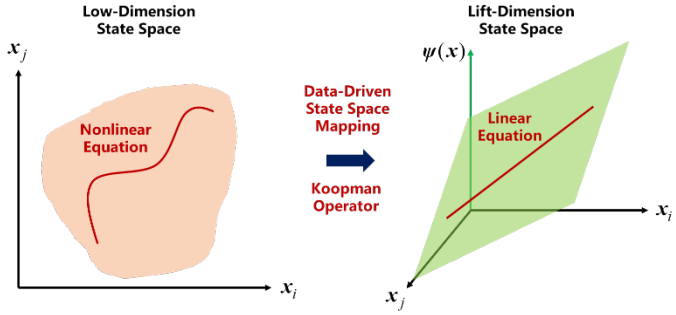

Fig. 2. KOT-based state space mapping.

According to the state equations in Section II, it can be concluded that the dynamic process of wind farms is mainly concerned with WT rotor speed and system frequency. With a constant regulation time and pre-set dead zone, the frequency response dynamic process under a severe load fluctuation can be expressed by $K_{f,sys}$. Meanwhile, the variation of WT rotor speed mainly depends on the WT rotor speed, frequency, and control variables $K_{f,i,n}$, $v_{w,i,n}$ and $K_{f,sys}$. Therefore, the nonlinear dynamic model of a wind farm can be formulated as

$$\boldsymbol{\omega}_i(t+1) = \varphi(\boldsymbol{\omega}_i(t),\ \boldsymbol{u}_i) \tag{21}$$

$$\boldsymbol{u}_i = [\boldsymbol{K}_{f,i},\ \boldsymbol{v}_{w,i},\ K_{f,sys}]^T \tag{22}$$

where $\boldsymbol{\omega}_i(t) \in \mathrm{R}^{N_i}$ denotes the vector composed of $\omega_{i,n}(t)$, whose dimension is N_i, $\boldsymbol{u}_i \in \mathrm{R}^{2N_i+1}$ denotes the control vector composed of $\boldsymbol{K}_{f,i}$ and $\boldsymbol{v}_{w,i}$, $\boldsymbol{K}_{f,i} \in \mathrm{R}^{N_i}$ and $\boldsymbol{v}_{w,i} \in \mathrm{R}^{N_i}$ denote the vector composed of $K_{f,i,n}$ and $v_{w,i,n}$ respectively, and $\varphi : \mathrm{R}^{3N_i} \to \mathrm{R}^{N_i}$ denotes the nonlinear relationship.

Based on the Koopman operator, the nonlinear relationship (21) can be mapped into a linear equation. We first define $\phi : \mathrm{R}^{3N_i} \to \mathrm{R}^{N_{i,lift}+2N_i+1}$ as the augmented input variable function, and $\boldsymbol{\xi} : \mathrm{R}^{2N_i+1} \to \mathrm{R}^{M}$ as the nonlinear augmented-dimension mapping function with M dimension:

$$\begin{aligned}\phi(\boldsymbol{\omega}_i(t), \boldsymbol{u}_i) &= [\boldsymbol{\omega}_i(t), \boldsymbol{\xi}(\boldsymbol{\omega}_i(t), \boldsymbol{v}_{w,i}, K_{f,sys}), \boldsymbol{u}_i]^{\mathrm{T}} \\ &= [\boldsymbol{z}_i(t), \boldsymbol{u}_i]^T\end{aligned} \tag{23}$$

where $\boldsymbol{z}_i(t) \in \mathrm{R}^{N_{i,lift}}$ denotes the augmented observation state of the i-th wind farm at time step t whose dimension is $N_{i,lift}$.

In order to guarantee the solvability of state space mapping model, this paper adopts a partial state space mapping in (23) where $\boldsymbol{\xi}$ is exclusive of $\boldsymbol{K}_{f,i}$, and can be expressed by scalar function:

$$\boldsymbol{\xi}(\boldsymbol{\omega}_i(t), \boldsymbol{v}_{w,i}, K_{f,sys}) = \begin{bmatrix} \xi_1(\boldsymbol{\omega}_i(t), \boldsymbol{v}_{w,i}, K_{f,sys}) \\ \vdots \\ \xi_M(\boldsymbol{\omega}_i(t), \boldsymbol{v}_{w,i}, K_{f,sys}) \end{bmatrix} \tag{24}$$

where $\xi_M : \mathrm{R}^{2N_i+1} \to \mathrm{R}$ denotes the M-th augmented-dimension mapping scalar function.

The mapping function has multiple typical forms. Due to the remarkable nonlinear fitting capability, 'polyharmonic' function is adopted in this paper, of which the m-th mapping scalar function can be defined as

$$\begin{cases} r_{i,m}(t) = \left\| \boldsymbol{x}_i(t) - \boldsymbol{c}_{i,m} \right\|_2^2 \\ \xi_m(\boldsymbol{\omega}_i(t), \boldsymbol{v}_{w,i}, K_{f,sys}) = r_{i.m}(t)^2 \log r_{i,m}(t) \end{cases} \tag{25}$$

where $\|\bullet\|_2^2$ denotes the Euclidean norm, $r_{i,m}(t)$ denotes the m-th Euclidean distance of i-th wind farm at step t, $\boldsymbol{x}_i(t)$ denotes the variables which implement partial state space mapping at t, expressed as $[\boldsymbol{\omega}_i(t), \boldsymbol{v}_{w,i}, K_{f,sys}]^T$, and $\boldsymbol{c}_{i,m} \in \mathrm{R}^{2N_i+1}$ denotes the m-th base vector of the i-th wind farm, whose elements are random within the range of $\boldsymbol{x}(t)$.

With $\boldsymbol{\xi}$ and ϕ, there must exist a linear model [23], which can be defined as

$$[\boldsymbol{\omega}_i(t+1), \boldsymbol{\xi}(\boldsymbol{\omega}_i(t+1), \boldsymbol{v}_{w,i}, K_{f,sys})] = \boldsymbol{K}_i \phi(\boldsymbol{\omega}_i(t), \boldsymbol{u}_i) \quad (26)$$

where $\boldsymbol{K}_i \in \mathrm{R}^{(N_{i,lift}+2N_i+1)\times N_{i,lift}}$ denotes the finite-dimensional approximate matrix of the infinite-dimensional Koopman operator of *i*-th wind farm, which can be partitioned as

$$\boldsymbol{K}_i = [\boldsymbol{A}_i \quad \boldsymbol{B}_i] \quad (27)$$

where $\boldsymbol{A}_i \in \mathrm{R}^{N_{i,lift}\times N_{i,lift}}$ denotes the $N_{i,lift} \times N_{i,lift}$ dimensional coefficient matrix corresponding to $z_i(t)$, $\boldsymbol{B}_i \in \mathrm{R}^{N_{i,lift}\times(2N_i+1)}$ denotes the $N_{i,lift} \times (2N_i+1)$ dimensional coefficient matrix corresponding to $\boldsymbol{u}_k$.

With (23) and (27), the linear (26) is reformatted as linear predictor form:

$$z_i(t+1) = \boldsymbol{A} \cdot z_i(t) + \boldsymbol{B} \cdot \boldsymbol{u}_i \quad (28)$$

2) Offline Training of Linear Coefficients Matrix

Since each wind farm's historical samples can be obtained, we define a training set as

$$\begin{cases} \mathbf{X}_i = [z_{i,1}(t), ..., z_{i,L}(t)], \mathbf{U}_i = [\boldsymbol{u}_{i,1}, ..., \boldsymbol{u}_{i,L}] \\ \mathbf{Y}_i = [z_{i,1}(t+1), ..., z_{i,L}(t+1)] \end{cases} \quad (29)$$

where $\mathbf{X}_i$ denotes the input variable sample set of the *i*-th wind farm, $\mathbf{U}_i$ denotes the control variable sample set of the *i*-th wind farm, $\mathbf{Y}_i$ denotes the output variable sample set of the *i*-th wind farm, and L denotes the number of samples.

In addition, the influence of sample noise on the state space mapping method is discussed in the author's previous research [27]. It should be noted that the training data set is unnecessary to come from continuous time series, and only needs to satisfy that each training sample can reflect the relationship between control parameters and rotor speed variation. Based on the training set, the matrix $\boldsymbol{A}_i$ and $\boldsymbol{B}_i$ is fitted by solving a least-square problem:

$$\min_{\boldsymbol{A}_i, \boldsymbol{B}_i} \left\| \mathbf{Y}_i - \boldsymbol{A}_i \cdot \mathbf{X}_i - \boldsymbol{B}_i \cdot \mathbf{U}_i \right\|_2^2 \quad (30)$$

The analytical solution to (30) is

$$[\boldsymbol{A}_i, \boldsymbol{B}_i] = \boldsymbol{G}_i^{\dagger} \mathbf{M}_i \quad (31)$$

where $[\bullet]^{\dagger}$ denotes the Moore-Penrose inverse, and $\boldsymbol{G}_i$, $\mathbf{M}_i$ are defined as

$$\boldsymbol{G}_i = \mathbf{Y}_i \begin{bmatrix} \mathbf{X}_i \\ \mathbf{U}_i \end{bmatrix}^T, \mathbf{M}_i = \begin{bmatrix} \mathbf{X}_i \\ \mathbf{U}_i \end{bmatrix} \begin{bmatrix} \mathbf{X}_i \\ \mathbf{U}_i \end{bmatrix}^T \quad (32)$$

B. Coordinated Data-Driven Assessment Model

Based on the derivation, the physical dynamic process is transformed into a data-driven linear form, and is shown in (33-b). The objective function in (17-a) can be rewritten in (33-a). The initial state of each wind farm augmented observation state is obtained by measurement, as shown in (33-c). The security constraints of WT rotor speed in (17-h) and nonnegative constraint in (17-i) can be rewritten as (33-e) and (33-d).

$$\mathbf{U}_i^* = \arg\max_{\{K_{f,i,n}\}} K_{f,i} = \left\| \boldsymbol{K}_{f,i} \right\|_1 = \sum_{i=1}^{N_I} \left| K_{f,i,n} \right| \quad (33\text{-a})$$

$$\begin{bmatrix} \boldsymbol{\omega}_i(t+1) \\ \boldsymbol{\xi}_i(t+1) \end{bmatrix} = \boldsymbol{A}_i \cdot \begin{bmatrix} \boldsymbol{\omega}_i(t) \\ \boldsymbol{\xi}_i(t) \end{bmatrix} + \boldsymbol{B}_i \cdot \begin{bmatrix} \boldsymbol{K}_{f,i} \\ \boldsymbol{v}_{w,i} \\ K_{f,sys} \end{bmatrix} \quad (33\text{-b})$$

$$z_i(0) = \left[\boldsymbol{\omega}_i(0), \boldsymbol{\xi}(\boldsymbol{\omega}_i(0), \boldsymbol{v}_{w,i}, K_{f,sys}) \right]^T \quad (33\text{-c})$$

$$\boldsymbol{K}_{f,i} \geq \mathbf{0} \quad (33\text{-d})$$

$$\boldsymbol{\omega}_{\min,i} \leq \boldsymbol{\omega}_i(t) \leq \boldsymbol{\omega}_{\max,i} \quad (33\text{-e})$$

where $\|\bullet\|_1$ denotes the L1-norm, and $\mathbf{0} \in \mathrm{R}^{N_i}$ denotes the zero vector whose dimension is N_i, $\boldsymbol{\omega}_{\max,i} \in \mathrm{R}^{N_i}$ and $\boldsymbol{\omega}_{\min,i} \in \mathrm{R}^{N_i}$ denote the vectors composed of $\omega_{\min,i,n}$ and $\omega_{\max,i,n}$, respectively, and (33-c) is the initial status condition of the linear model.

With (18) and (33), the iteration process in (19) can be rewritten as

$$\begin{cases} \text{Equ. (18)} \\ \begin{cases} \boldsymbol{K}_{f,1}(s+1) = \mathbf{U}_1^* \left(\boldsymbol{K}_{f,1}, K_{f,sys}(s+1) \right) \\ \boldsymbol{K}_{f,2}(s+1) = \mathbf{U}_2^* \left(\boldsymbol{K}_{f,2}, K_{f,sys}(s+1) \right) \\ \vdots \\ \boldsymbol{K}_{f,I}(s+1) = \mathbf{U}_I^* \left(\boldsymbol{K}_{f,I}, K_{f,sys}(s+1) \right) \end{cases} \end{cases} \quad (34)$$

To sum up, the data-driven state space mapping MPC assessment model of wind farm in (33), system coefficient update in (18), iteration process in (34), and convergence conditions (20) construct the completely coordinated data-driven assessment model, which is a convex optimization problem with inherent solvability.

C. Comprehensive Assessment Process of Wind Farm

Complete data-driven assessment process based on state space mapping and KOT can be divided into two stages: offline training and online assessment, as shown in Fig. 3.

The offline training process can be summarized as follows: 1) Obtain historical samples $\boldsymbol{\omega}_i(t)$, $\boldsymbol{\omega}_i(t+1)$, $\boldsymbol{K}_{f,i}$, $K_{f,sys}$, $\boldsymbol{v}_{w,i}$. 2) Determine the value of $\boldsymbol{c}_m$ and generate training sets $\mathbf{X}_i$, $\mathbf{Y}_i$, $\mathbf{U}_i$ of each wind farm, respectively. 3) Estimate the linear matrix $\boldsymbol{A}_i$ and $\boldsymbol{B}_i$ by (31) and construct state space mapping MPC model of each wind farm, respectively.

The online assessment process can be summarized as follows: 1) Input real-time wind speed measurement or predicted value, and initial WT rotor speed to (28). 2) Set $s = 0$, $\boldsymbol{K}_{f,i}(s) = \mathbf{0}$. 3) With $\boldsymbol{K}_{f,i}(s)$, grid dispatching center calculates $K_{f,sys}(s+1)$ by (18), and issues to all wind farms. 4) With the state space mapping MPC model, each wind farm assesses $\boldsymbol{K}_{f,i}(s+1)$ individually, and reports it to grid

dispatching center. 5) If $\boldsymbol{K}_{f,i}(s)$ and $K_{f,sys}(s)$ convergence, record $\boldsymbol{K}_{f,i}(s)$ as the optimal coefficients boundary of wind farms, or repeat steps 3-4.

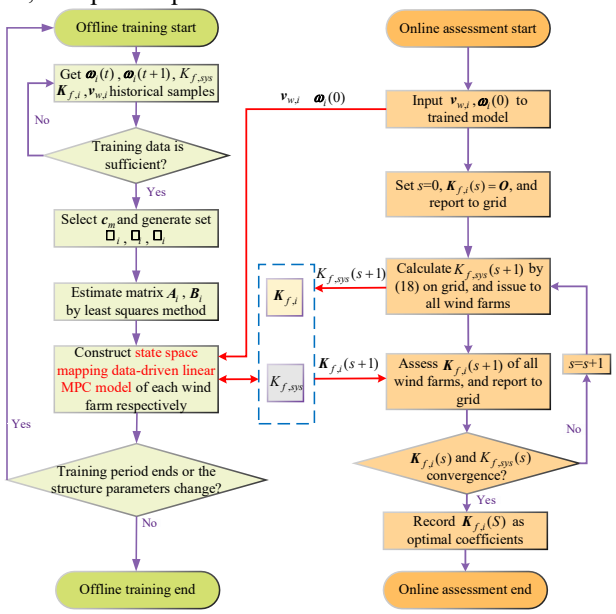

Fig. 3. Flow chart of assessment process based on state space mapping MPC.

IV. Case Study

In this section, case studies are carried out to validate the performance of the proposed assessment approach. A physical-based timing simulation model of the wind farm is also constructed and considered as a benchmark. In the test system, it contains three wind farms, of which installed capacities are 48 MW, 64MW and 80MW, composed of 12 WTs, 16WTs and 20 WTs, respectively. Each WT capacity is 4MW, and each anemometer in wind farms corresponds to 4 WTs. A severe system power mismatch is assumed to occur at the beginning of the PFR process. With a range from 7 to 11 m/s, 16 wind speed scenarios are used to carry out the test. It should be emphasized that the historical samples exclude the test scenarios. Complete simulation parameters of the physical-based timing simulation system, and data-driven training, are provided in [28], and 16 test wind speed scenarios is shown in Fig. 4-6:

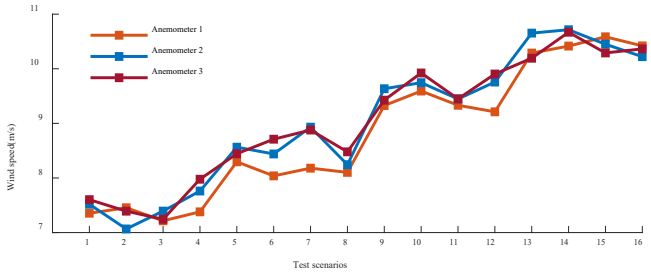

Fig. 4. Wind speed test scenarios of wind farm 1

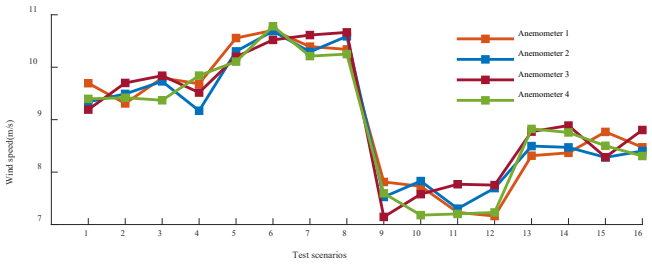

Fig. 5. Wind speed test scenarios of wind farm 2.

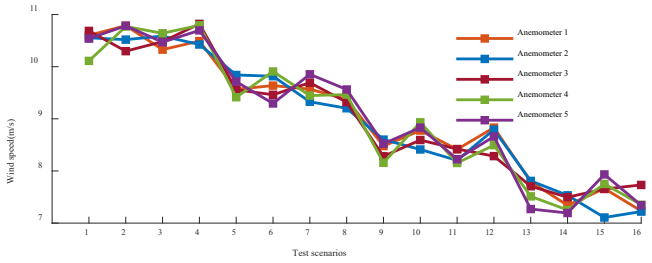

Fig. 6. Wind speed test scenarios of wind farm 3.

A. Optimal Coefficients Assessment

The assessment results $K_{f,i}$ of the proposed state space mapping MPC method with coordinated iteration is shown in Fig. 7 to Fig. 9. The assessed optimal coefficients of the coordinated iteration assessment model based on timing simulation with an accurate physical model are considered as the truth value. For comparison, the state space mapping MPC method with non-iteration, and timing simulation based on an inaccurate physical model, i.e., +6% derivation of blade radius and +6% derivation of rotational inertia is also carried out. The results shown in Fig. 7 to Fig. 9 suggest that PFR capability is intensely influenced by wind speed and WT status. In frequency-dropping scenarios, $K_{f,i}$ exhibits an uptrend with wind speed increasing, since higher wind speed implies wider downward regulation range of WTs. On the contrary, in frequency-rising scenarios, $K_{f,i}$ exhibit a downtrend with wind speed increasing, since the downward regulation implies the range is narrow.

Fig. 7 to Fig. 9 validate that once parameters are inaccurate, physical model methods definitely deviate from the real frequency regulation capability. Meanwhile, without performing coordinated iteration, the frequency regulation capability is inevitably less than the optimal result. The comparison demonstrates that the proposed method has the advantage of highly accurate assessment without relying on physical model parameters and the coordinated iteration can fully exploit and improve the wind farm PFR capability in PFR process.

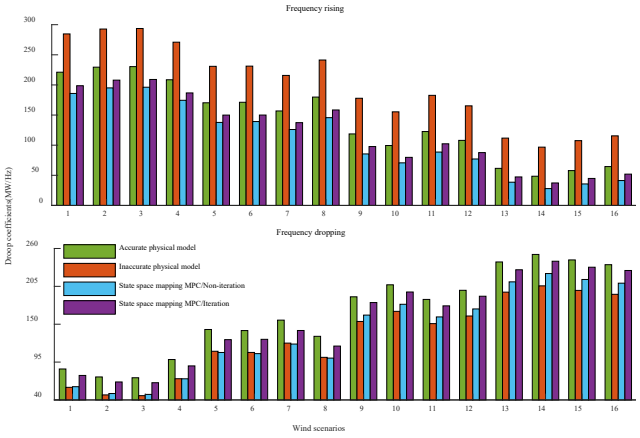

Fig. 7. Optimal droop coefficients assessment results of wind farm 1.

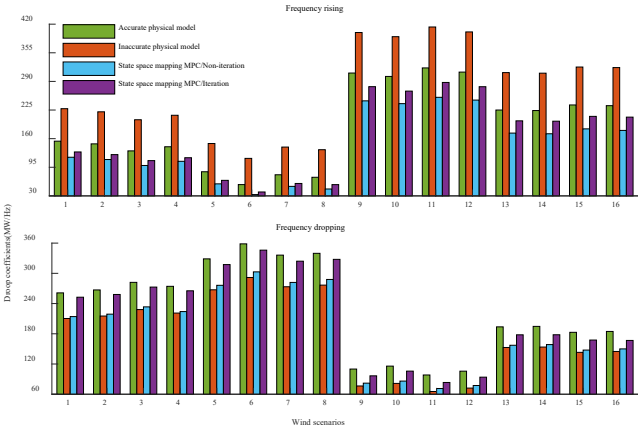

Fig. 8. Optimal droop coefficients assessment results of wind farm 2.

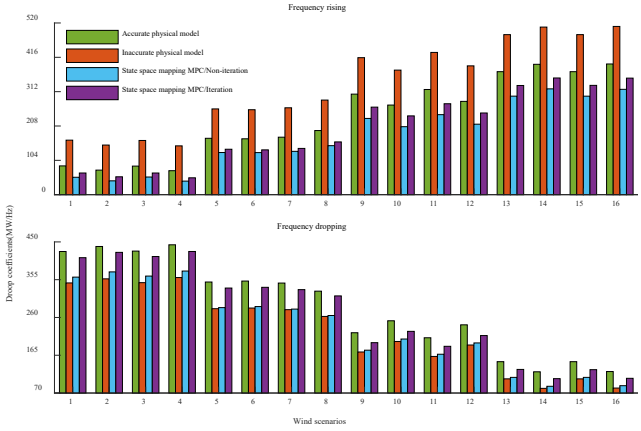

Fig. 9. Optimal droop coefficients assessment results of wind farm 3.

B. Analysis of Control Performance

Furthermore, this part uses assessment results as control parameters to carry out timing simulation, and observes the final rotor speed of WT after PFR in test scenarios. Maximum relative error (MRE) and root mean square error (RMSE) are used to analyze the deviation degree of WT rotor speed to their boundaries. To explicitly express, MRE1/RMSE1 in Fig. 10-11 represents the MRE or RMSE index of wind farm 1. As shown in Fig. 7 and Fig. 8, it can be concluded that the WT operation status under the proposed method is much closer to the boundary compared to the non-iteration state space mapping MPC and inaccurate physical model method. The comparison verifies that the control performance of the proposed method is independent of the parameters, and the PFR capability of WT is sufficiently exploited with coordinated iteration.

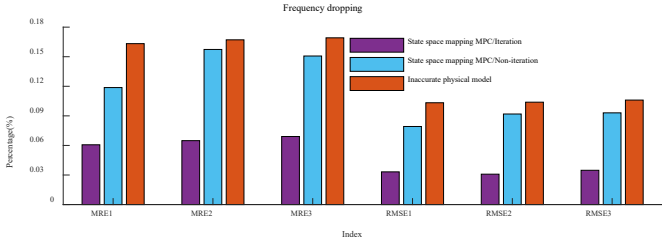

Fig. 10. Control accuracy of WT with assessment results in frequency dropping scenarios.

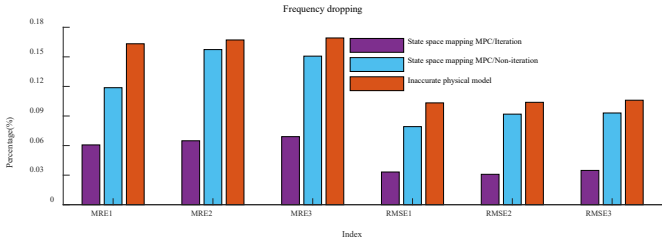

Fig. 11. Control accuracy of WT with assessment results in frequency rising scenarios.

C. Analysis of Data Quality Influence

TABLE I
INFLUENCE OF DATA QUALITY IN FREQUENCY RISING

Index	Index	Training set 1 (p.u.)	Training set 2 (p.u.)	Training set 3 (p.u.)
Wind farm 1	MRE	7.18E-02	6.73E-02	6.70E-02
	RMSE	3.77E-02	3.85E-02	3.22E-02
Wind farm 2	MRE	7.77E-02	6.84E-02	6.27E-02
	RMSE	3.91E-02	3.68E-02	2.76E-02
Wind farm 3	MRE	8.11E-02	7.14E-02	6.66E-02
	RMSE	4.20E-02	3.83E-02	2.75E-02

TABLE II
INFLUENCE OF DATA QUALITY IN FREQUENCY DROPPING

Index	Index	Training set 1 (p.u.)	Training set 2 (p.u.)	Training set 3 (p.u.)
Wind farm 1	MRE	5.96E-02	6.07E-02	6.42E-02
	RMSE	3.19E-02	3.32E-02	3.47E-02
Wind farm 2	MRE	6.24E-02	6.49E-02	7.08E-02
	RMSE	2.99E-02	3.09E-02	3.37E-02
Wind farm 3	MRE	6.82E-02	6.91E-02	7.51E-02
	RMSE	3.18E-02	3.48E-02	3.98E-02

In addition, we further discuss the influence of the range of training set. Three training sets with different WT rotor speed ranges are discussed: training set 1 with a rotor speed range of [0.7,1.3] p.u., training set 2 with a rotor speed range of

[0.73,1.27] p.u., and training set 3 with a rotor speed range of [0.76,1.24] p.u..

As shown in Table I and Table II, with a wider rotor speed range of the training set, the MRE and RMSE of assessment results between the proposed method and timing simulation are smaller, both in frequency rising and dropping scenarios. Nevertheless, it can be concluded that, since the global linearity of the state space, training set 2 also can keep the MRE within 7.14E-02 p.u. in most scenarios. It demonstrates that rotor speed approaching to boundary is unnecessary to be covered in training set, since the proposed method can has the advantage of global linear characteristic.

D. Analysis of Coordinated Iteration

TABLE III
NUMBER OF ITERATIONS IN ALL TEST SCENARIOS

Index	State space mapping MPC	Timing simulation
Frequency rising	6	8
Frequency dropping	6	6

TABLE IV
AVERAGE ASSESSMENT TIME OF PROPOSED METHOD

Index	Wind farm 1	Wind farm 2	Wind farm 3
Offline training(s)	10.352	12.04	14.192
Online assessment(s)	7.456	8.896	10.184

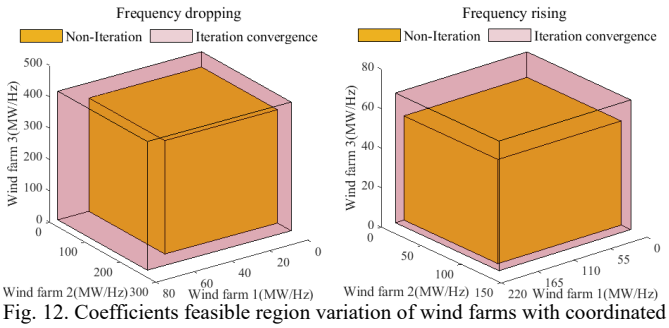

Fig. 12. Coefficients feasible region variation of wind farms with coordinated iteration.

We further discuss the effect of coordinated iteration process. As shown in Table III, it can be concluded that the proposed coordinated iteration method exhibits satisfactory convergence performance in all wind speed conditions. Meanwhile, the average time of assessment process is an important index to evaluate the method. The average online assessment time of the proposed coordinated iteration is shown in Table IV, which is less than 10.2 s. The results suggest that the proposed method has the merit of fast analytical solving, and guarantees real-time application since the rolling assessment is usually implemented at minutes level. Moreover, as shown in Table IV, the offline training can be finished with no need for long training time.

The feasible region variation of wind farm coefficients with coordinated iteration is shown in Fig. 12. We choose wind speed scenario 1 for test, and Fig. 12 also shows coefficient feasible region under state space mapping MPC without coordinated iteration. Compared to non-iteration results, it can be concluded that the coefficient boundary is significantly extended by coordinated iteration.

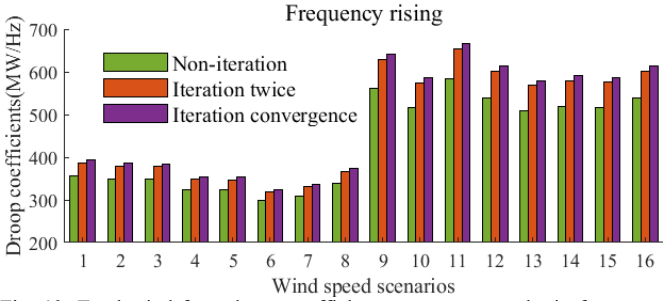

Fig. 13. Total wind farm droop coefficient assessment results in frequency rising scenarios.

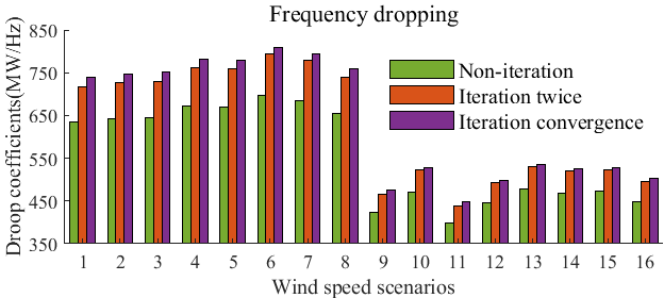

Fig. 14. Total wind farm droop coefficient assessment results in frequency dropping scenarios.

In addition, the variation of K_f with coordinated iteration is shown in Fig. 12 and Fig. 14. For comparison, state space mapping MPC without iteration, with twice iteration and converged iteration are carried out to assess the optimal coefficients of wind farms, respectively. Fig. 13 and Fig. 14 illustrate that K_f is also significantly increased with the iteration, and the assessment results with twice iteration are closer to the converged results. In order to reduce communication time, the proposed method can only implement twice iteration for real application. Furthermore, the average relative increase rate (ARIR) is used to analyze the degree of improvement of K_f and $K_{f,i}$ by coordinated iteration in all test scenarios. As shown in Table V, both K_f and $K_{f,i}$ increase more than 10% by coordinated iteration in frequency rising and dropping scenarios. The results in Fig. 12 to Fig. 14 and Table V further demonstrate that the proposed coordinated iteration process has the significant advantage of remarkably exploiting and improving PFR capability for the power system and each wind farm.

TABLE V
COEFFICIENTS ARIR OF WIND FARMS

	K_f	$K_{f,1}$	$K_{f,2}$	$K_{f,3}$
ARIR in frequency dropping scenarios	14.18%	16.80%	16.13%	15.23%
ARIR in frequency rising scenarios	11.69%	14.10%	13.80%	14.52%

E. Analysis of PFR Dynamic Process

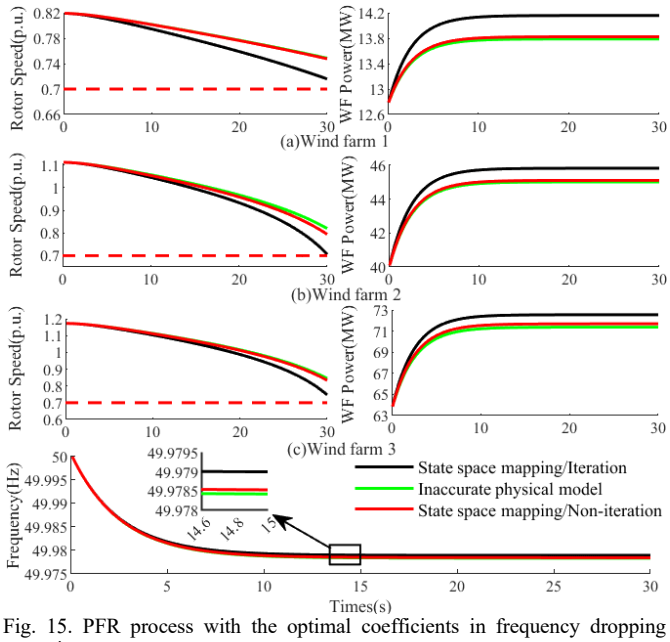

Fig. 15. PFR process with the optimal coefficients in frequency dropping scenarios.

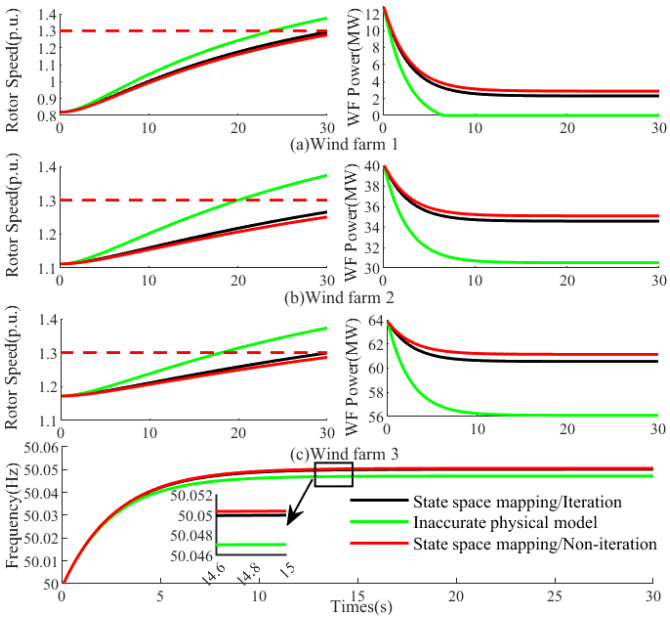

Fig. 16. PFR process with the optimal coefficients in frequency rising scenarios.

Furthermore, to validate the assessment performance, we use the optimal coefficients as control parameters and analyze the PFR dynamic process. For comparison, the results under the inaccurate physical model and non-iteration state space mapping MPC are also given. Wind speed scenario 3 is used to test the PFR dynamic process.

As shown in Fig. 15 and Fig. 16, under the proposed method, the WT rotor speed is closer to the boundary, and power output of wind farm in the overall PFR process is effectively improved. By contrast, using the coefficients obtained from inaccurate parameters or non-iteration state space mapping MPC, the rotor speed and power output exceed the corresponding limits, or insufficiently use the regulation capability in the PFR process. In addition, this research focuses on the PFR and the speed recovery period is not included. Therefore, a truncation time is considered in Fig. 15 and Fig. 16, which fully utilized the WT kinetic energy and rotor speed reach boundary after PFR. The results verify that the proposed method can adequately exploit the WTs' PFR capability, prevent rotor speed and power output from exceeding security boundaries, and ensure the safety of wind farm PFR.

V. Conclusion

In this paper, a data-driven state space mapping MPC method considering coordinated iteration between grid dispatching center and multiple wind farms is proposed to assess the maximum PFR capability of each wind farm. Based on the KOT, the original physical-based dynamic model of wind farm PFR is mapped onto a global linear pattern in augmented state space by only using historical samples in offline training. Based on the state space mapping linear MPC, this paper constructs a convex optimization model to precisely assess the feasible region boundary of wind farm PFR capability. Furthermore, with the coordinated iteration framework, the PFR capability of wind farms is significantly improved and obtains the optimal coefficient feasible region boundary.

The simulation results verify that the proposed method has remarkable advantages over the physical-based method and non-iteration method. In particular, the proposed method is independent of model completeness and parameter accuracy, decreases the demand for training samples, achieves fast analytical solution in real-time, and significantly enhances the PFR capability of wind farms and power system.

References

[1] M. Lu, C. Chang, W. Lee, and L. Wang, "Combining the wind power generation system with energy storage equipment," *IEEE Trans. Ind. Appl.*, vol. 45, no. 6, pp. 2109-2115, Nov-Feb. 2009.

[2] W. Tang, J. Hu, Y. Chang, and F. Liu, "Modeling of DFIG-based wind turbine for power system transient response analysis in rotor speed control timescale," *IEEE Trans. Power Syst.*, vol. 33, no. 6, pp. 6795-6805, Nov. 2018.

[3] D. Li, W. Yan, W. Li, and Z. Ren, "A two-tier wind power time series model considering day-to-day weather transition and intraday wind power fluctuations," *IEEE Trans. Power Syst.*, vol. 31, no. 6, pp. 4330-4339, Nov. 2016.

[4] M. Rahimi, "Dynamic performance assessment of DFIG-based wind turbines: A review," *Renewable Sustainable Energy Rev.*, vol. 37, pp. 852-866, June 2014.

[5] A. Teninge, C. Jecu, D. Roye, S. Bacha, J. Duval and R. Belhomme,"Contribution to frequency control through wind turbine inertial energy storage," *IET Ren. Power Gen,* vol.3, no.3, pp.358-370,. 2009.

[6] K. V. Vidyanandan, N. Senroy, "Primary frequency regulation by deloaded wind turbines using variable droop," *IEEE Trans on Power Sys,* vol.28, no.2, pp.837-846, May 2013.

[7] M. Kayikçi and J. V. Milanovic, "Dynamic contribution of DFIG-

based wind plants to system frequency disturbances," *IEEE Trans. Power Syst*., vol. 24, no. 2, pp. 859-867, May 2009.
[8] J. Morren, S. W. De Haan, W. L. Kling, and J. Ferreira, "Wind turbines emulating inertia and supporting primary frequency control," *IEEE Trans. Power Syst.*, vol. 21, no. 1, pp. 433-434, Feb. 2006.
[9] I. D. Margaris, S. A. Papathanassiou, N. D. Hatziargyriou, A. D. Hansen, and P. Sorensen, "Frequency control in autonomous power systems with high wind power penetration," *IEEE Trans. Sustainable Energy,* vol. 3, no. 2, pp. 189-199, Mar. 2012.
[10] H. Ye, W. Pei, and Z. Qi, "Analytical modeling of inertial and droop responses from a wind farm for short-term frequency regulation in power systems," *IEEE Trans. Power Syst.*, vol. 31, no. 5, pp. 3414-3423, Sept. 2016.
[11] L. M. Castro and E. Acha, "A new method to assess the contribution of VSC-HVDC connected wind farms to the primary frequency control of power networks," *Electr. Power Syst. Res.*, vol. 154, pp. 48-58, Sept. 2018.
[12] Y. K. Wu, W. H. Yang, Y. L. Hu, and P. Q. Dzung, "Frequency regulation at a wind farm using time-varying inertia and droop controls," *IEEE Trans. Ind. Appl*., vol. 55, no. 1, pp. 213-224, Jan. 2019.
[13] F. Teng, V. Trovato, and G. Strbac, "Stochastic scheduling with inertia-dependent fast frequency response requirements," *IEEE Trans. Power Syst.*, vol. 31, no. 2, pp. 1557-1566, Apr. 2016.
[14] F. Teng and G. Strbac, "Assessment of the role and value of frequency response support from wind plants," *IEEE Trans. Sustainable Energy*, vol. 7, no. 2, pp. 586-595, Apr. 2016.
[15] Q. Wang, F. Li, Y. Tang, and Y. Xu, "Integrating model-driven and data-driven methods for power system frequency stability assessment and control," *IEEE Trans. Power Syst.*, vol. 34, no. 6, pp. 4557-4568, Nov. 2019.
[16] P. Kou, D. Liang, L. Yu, and L. Gao, "Nonlinear model predictive control of wind farm for system frequency support," *IEEE Trans. Power Syst.,* vol. 34, no. 5, pp. 3547-3561, Feb. 2019.
[17] X. Lyu, Y. Jia and Z. Dong, "Adaptive frequency responsive control for wind farm considering wake interaction," *J. Mod. Power Syst. Clean Energy*, vol. 9, no. 5, pp. 1066-1075, Sept. 2021.
[18] Z. Hou and S. Xiong, "On model-free adaptive control and its stability analysis," *IEEE Trans. Autom. Control*, vol. 64, no. 11, pp. 4555-4569, Nov. 2019.
[19] W. Jiang and J. P. Lu, "Frequency estimation in wind farm integrated systems using artificial neural network," *Int. J. Electr. Power Energy Syst.*, vol. 62, pp. 72-79, Nov. 2014.
[20] M. Kheshti, L. Ding, W. Bao, M. Yin, Q. Wu, and V. Terzija, "Toward intelligent inertial frequency participation of wind farms for the grid frequency control," *IEEE Trans. Ind. Inf.*, vol. 16, no. 11, pp. 6772-6786, Nov. 2020.
[21] Y. Liang, X. Zhao, and L. Sun, "A multiagent reinforcement learning approach for wind farm frequency control," *IEEE Trans. Ind. Inf.*, vol. 19, no. 2, pp. 1725-1734, Feb. 2023.
[22] X. Yin and X. Zhao, "Deep neural learning based distributed predictive control for offshore wind farm using high-fidelity LES data," *IEEE Trans. Ind. Electron.*, vol. 68, no. 4, pp. 3251-3261, Apr. 2021.
[23] M. Korda and I. Mezic, "Linear predictors for nonlinear dynamical systems: Koopman operator meets model predictive control," *Automatica*, vol. 93, pp 149-160, July. 2018.
[24] B. O. Koopman, "Hamiltonian systems and transformation in Hilbert space," *PNAS*, vol. 17, no. 5, p. 315, Mar. 1931.
[25] Y. Enoch, K. Soumya, H. Nathan, "Learning deep neural network representations for Koopman operators of nonlinear dynamical systems," *2019 American Control Conference* (ACC), Philadelphia, PA, USA, 2019, pp 10-12.
[26] Z. Chu, U. Markovic, G. Hug, and F. Teng, "Towards Optimal System Scheduling With Synthetic Inertia Provision From Wind Turbines," *IEEE Trans. Power Syst.*, vol. 35, no. 5, pp. 4056-4066, Sept. 2020.
[27] L. Guo, Y. Zhang, X. Li, Z. Wang, Y. Liu, L. Bai, *et al*.,"Data-driven power flow calculation method: a lifting dimension linear regression approach," *IEEE Trans. Power Syst.*, vol. 37, no. 3, pp. 1798-1808, May 2022.
[28] Complete simulation parameters. [Online]. Available: https://drive.google.com/file/d/1bwElfHa80YqPtVYBKyh9Vx3gm3Jjoj4v/view?usp=sharing